Low-voltage shock-mitigated micro-electromechanical systems structure

Ang Chen, Suhyun Nam, Ying-Cheng Lai, and Junseok Chae

Citation: Appl. Phys. Lett. **110**, 201903 (2017); doi: 10.1063/1.4983645
View online: http://dx.doi.org/10.1063/1.4983645
View Table of Contents: http://aip.scitation.org/toc/apl/110/20
Published by the American Institute of Physics

Low-voltage shock-mitigated micro-electromechanical systems structure

Ang Chen, Suhyun Nam, Ying-Cheng Lai, and Junseok Chae
School of Electrical, Computer, and Energy Engineering, Arizona State University, Tempe, Arizona 85287, USA

(Received 15 November 2016; accepted 4 May 2017; published online 16 May 2017)

We report a low-voltage, yet effective, micro-electromechanical systems (MEMS) structure capable of mitigating external mechanical disturbances, such as a physical shock. External shock onto MEMS devices can be catastrophic as a conventional single membrane may travel beyond stable oscillatory distances under shock and become irreparably damaged. However, the simple addition of a second membrane on top of the single membrane drastically reduces oscillatory distances by electrostatically holding the bottom membrane within stable oscillation. The added elements, in conjunction with a fine-control algorithm, mitigate the impact of a mechanical shock onto the MEMS device. From experimental findings, it is found that the dual-membrane structure effectively reduces the travel distance of the bottom membrane by 41.5%, upon deploying merely 0.565 V onto the additional membrane. The dynamic implementation of the shock mitigation method, using an on-board accelerometer as a trigger, delivered *in-situ* mitigation of shock on a dual-membrane MEMS structure. *Published by AIP Publishing.*
[http://dx.doi.org/10.1063/1.4983645]

Micro-electromechanical systems (MEMS) devices have infiltrated many applications, including the emerging field of drug delivery,[1] sensors, and actuators in the automotive industry,[2] such as accelerometers to deploy airbags,[3] gyroscopes for stability control of mobile electronics,[4] and many others.[5–10] MEMS devices contribute the core components of these high-tech products used daily. Consequently, the reliability of MEMS devices becomes a critical factor that must be reconciled.

Characterized by their highly miniaturized size and facile fabrication process, MEMS devices are widely used in multi-physics environments, exposing them to mechanical, thermal, chemical, and other disturbances. Among them, one of the most critical issues affecting the reliability of MEMS devices is the external mechanical shock. An external mechanical shock can be defined as a sudden force over a short period applied on the MEMS device relative to the natural frequency of the structure. It can cause cracking, chipping, and fracture due to the highly induced loads on the structure,[11] which is a key factor to be considered in the design stage of MEMS devices.[12] MEMS structures are subjected to external mechanical shocks during fabrication, deployment, or operation.[13] In certain situations, a MEMS device can be subjected to an extreme shock-load magnitude of greater than 2×10^4 g (g is the acceleration of gravity, 9.81 m/s^2). If severe enough, it can cause irreversible damage to devices.[14] Without a proper mitigation mechanism, the overall system functionality can be affected by severe deformation of the microstructure.[12] Furthermore, exposure of MEMS structures to dynamic loads due to mechanical shock can also cause mechanical and electrical failures,[11] such as the stiction of micro-beams[15] and short circuit of capacitors,[14] respectively. In hard disk drives, an unexpected drop may result in damaging of the MEMS actuator, affecting the bandwidth of servo tracking and fine positioning of the magnetic head.[16] Other well-developed portable devices contain MEMS structures, which re-emphasize the requirement for reliability against shock.[17]

Investigation into the protection of MEMS devices from external shock has led to multiple findings. Srikar *et al.* explored a theoretical analysis of the reliability of MEMS under shock, evaluating shocks in the form of elastic waves, vibration, and quasi-static oscillation in terms of the overall shock duration.[13] Younis *et al.* reported an efficient computational model of the dynamic response MEMS structures under shock.[18] The development of a general method for modeling the reliability of MEMS devices established a reference for the predicted maximum acceleration of vibration and maximum shock based on the frequency and the pulse length.[19] Yang *et al.* also dynamically analyzed the drop-shock of the MEMS/Package system.[20]

While many theoretical and experimental studies of MEMS shock responses have been explored, only a small number of prior studies have attempted to mitigate the impact of shock. Wilner *et al.* reported hard shock stops as a mitigation method; however, these physical structures tended to generate secondary impacts and cause undesirable device oscillations.[21] Yoon *et al.* suggested nonlinear springs and soft coatings in order to improve shock mitigation.[22] Weber *et al.* presented adaptive control to reduce vibration-induced bias errors in inertial sensors.[23] These attempts require sophisticated structures and algorithms to implement and are less effective and sensitive upon implementation than structures without shock mitigating features.

To overcome some of these challenges, we present a dual-membrane MEMS structure that can effectively mitigate shock using electrostatic stimuli in conjunction with inherent restoration force. Although the electrostatic force has been used to stabilize MEMS structures for years, this method focuses on anti-phase synchronization. Our previous work on the anti-phase synchronization showed the effective reduction of free-moving membranes against external

impulsive disturbances, i.e., shock, using detailed mathematical analysis.[24] Our method aims to demonstrate the anti-phase synchronization for the effective reduction of two free-moving membranes against shocks, all in experimental practical settings. Comparing a conventional MEMS configuration, i.e., a structure with a movable membrane and a fixed substrate [Fig. 1(a)], with a shock mitigating dual membrane structure [Fig. 1(b)] allows us to perform a side-by-side analysis of the shock responses of these structures. The dual-membrane structure effectively prevents the movable bottom membrane from traveling beyond the allowed distance by simply adding a second thin-film membrane on top of it. This structure effectively reduces the bottom membrane travel distance by 41.5%, upon deploying merely 0.565 V onto the additional membrane under *ex-situ* control and 56% by applying 1.72 V under *in-situ* dynamic control. Therefore, this shock mitigating technique can be applied throughout the field of MEMS to drastically decrease the shock impact on micro-speakers, capacitive actuators, harsh environmental sensors, and other transducers.

The fabrication process to develop the dual-membrane structure supports CMOS-compatible technology. The first step required a 400-nm-thick silicon nitride layer to be deposited by plasma-enhanced chemical vapor deposition (PECVD) for isolation. To make a silicon substrate contact, a 3 μm silicon nitride layer was removed by fluorine-based reactive-ion etching (RIE) (CF_4: 50 sccm, O_2: 5 sccm, pressure: 50 mTorr, and power: 150 W). It was followed by a 4-μm-thick silicon dioxide deposition by PECVD for the first sacrificial layer. The bottom membrane is composed of three layers: a 200-nm-thick silicon nitride layer for isolation from the substrate, a 1-μm-thick highly doped polysilicon, and another 400-nm-thick silicon nitride for the isolation between membranes. We defined the bottom membrane, as well as air-venting holes, using fluorine-based RIE (Si_3N_4/Polysilicon: CF_4: 50/30 sccm, O_2: 5/10 sccm, pressure: 50/175 mTorr, and power/RF power: 150/50 W). Then, a 4-μm-thick second sacrificial layer of silicon dioxide, followed by the top membrane, was deposited. The top membrane consists of two layers: 200-nm-thick PECVD silicon nitride and 1-μm-thick low pressure chemical vapor deposition (LPCVD) highly doped polysilicon. To form the air-venting holes, fluorine-based RIE was used to etch the top membrane (Polysilicon/Si_3N_4). Thin-film layers of Cr/Au (20/200 nm) form electrical contacts with the top membrane, bottom

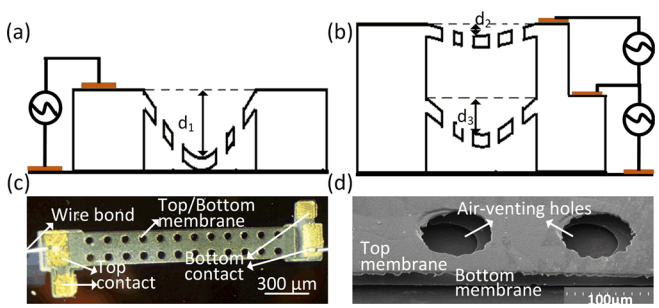

FIG. 1. (a) A conventional single movable membrane upon shock. (b) Dual-membrane structure with an additional top membrane and a movable bottom membrane upon shock. (c) Top view of the fabricated dual-membrane device. (d) Cross-sectional view of the fabricated dual-membrane device.

membrane, and substrate, which are then connected to external readout using wire bonds. The dual membranes are free to move once the two sacrificial layers were etched by a 10% hydrofluoric acid solution. Figures 1(c) and 1(d) exhibit the top and the cross-sectional views of a dual membrane structure, respectively.

A custom-made drop test apparatus [Fig. 2(a)] was constructed to evaluate the shock-mitigated MEMS structures. Four vertical steel pillars support a wooden drop platform with dimensions of $0.6 \times 14 \times 31$ cm at a given height, i.e., 15 cm or 22 cm, from the hard floor. A stopper (small cylindrical wooden pin) pins the platform and when removed will cause the test board on the platform to drop perpendicular to the floor. Rubber bands were incorporated at the end of the platform, to enhance the rapid drop of the MEMS structures and consequently reduce the friction between the platform and the test board. When the test board drops at a given height and hits the floor, the shock load corresponding to the inertia applies to the MEMS structures on the board. The fabricated device was mounted in a dual inline package (Spectrum Semiconductor Materials, Inc., HYB02415), and a readout circuit was assembled on the custom-made test board as shown in Fig. 2(b). USB-6210 DAQ from National Instrument collects the resulting data at output of the readout using a sampling frequency of 50 kHz, and MATLAB processes the data using signal analysis with a Butterworth digital filter. This filter spans from 500 Hz to 1500 Hz in order to isolate the shock response signal.

Figure 2(c) shows the simplified schematic of readout, including a high pass filter with a gain of 21 dB in order to remove low frequency noise. Two variable capacitors model the MEMS structures, followed by a trans-impedance amplifier, including the precision operational amplifier, ALD1702 (Advanced Linear Devices Inc. $R1 = 1\,M\Omega$, $R2 = 1\,k\Omega$, $R3 = 11\,k\Omega$, and $C = 1$ mF). The readout circuit, a commercial accelerometer (MMA1200KEG, Freescale Inc.), and systems were all assembled on the test board.

A control was established that the output of the MEMS structures was recorded upon a given shock without applying electrostatic force between the top and bottom membranes. The silicon substrate was biased at –2 V, while maintaining zero voltage difference between the top and bottom membranes. The test board was dropped at 22 cm and hit a hard surface, delivering approximately 100 g to the MEMS structures, as measured by the on-board accelerometer. To evaluate the effectiveness of the shock mitigation, we collected outputs of MEMS structures upon a shock at different values of electrostatic forces, i.e., DC voltage, applied between the top and bottom membranes.

To implement an *in-situ* control of electrostatic force, a microcontroller and an accelerometer were used to control the timing of electrostatic force upon a shock. When the output of the accelerometer exceeded a threshold of 1.16 V, the micro-controller sent a command to apply an electrostatic force within the peak shock amplitude period of around 500 μsec (200 μsec Fig. 2(d)). The force was applied between the top and bottom membranes in order to mitigate the shock effect before the bottom membrane reaches its maximum travel distance. Thus, the timing scheme prevented the bottom membrane from hitting the substrate. To evaluate the

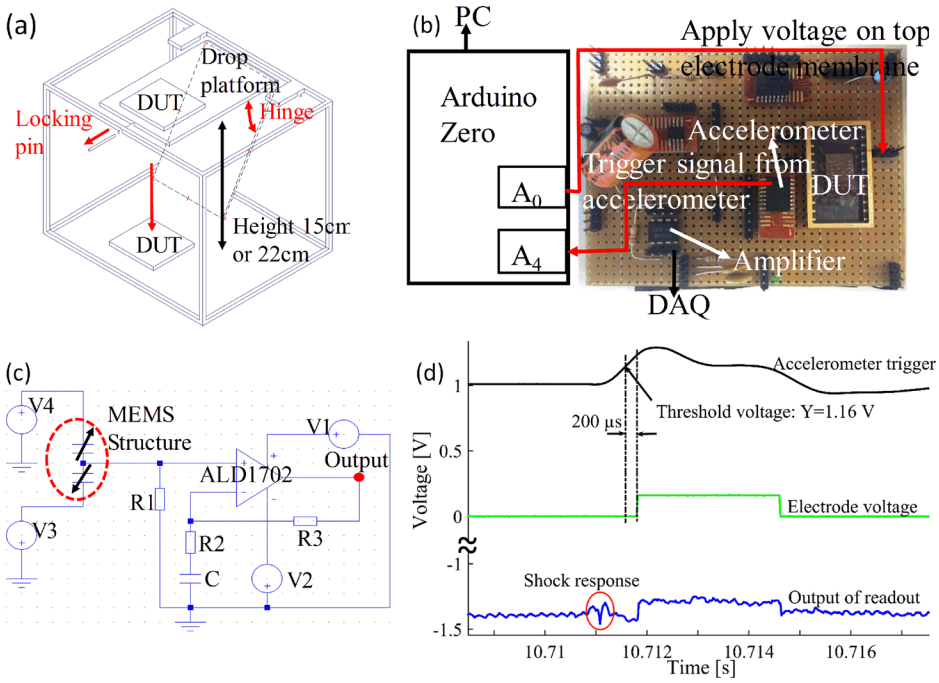

FIG. 2. Experimental setup: (a) Schematic of the drop setup; a pin holds the drop platform and releases it to drop the test board to the hard floor. The adjustable travel distance is set to be 22 cm, and the corresponding shock load is ~100 g. (b) Micro-controller board and test board. (c) Simplified schematic of the readout circuit. (d) Temporal profiles of the accelerometer, electrode voltage, and output of readout with a shock load of 100 g.

effectiveness of *in-situ* control, we dropped the board containing an accelerometer trigger and a microcontroller. The *in-situ* control not only capably implemented electrostatically mitigation but also had no influence on the identification of the shock response of the microstructure in the presence of the shock impact. Once the microstructure experienced the shock impact, we easily distinguished the shock response in the time domain.

To emulate more realistic settings, such as dropping a cell phone with ambient noise, we repeated the above protocol in the presence of an acoustic stimulus. We placed a loudspeaker at a distance of 1.6 cm above the DUT to impose an acoustic excitation of 98 dB sound pressure level (SPL) (calibrated by a SPL Meter, CM-130 by Galaxy Audio Company) and performed the drop protocol. The MEMS device along with its readout circuit was dropped from the same conditions, and LabVIEW Signal Express visualized the temporal profiles of the accelerometer, the voltage of the top membrane, and the readout circuit.

We investigated the responses of MEMS devices under a combination of shock loads and electrostatic actuation. MEMS devices typically employ capacitive changes, corresponding to the movement of the movable membrane. The performance of shock-mitigated MEMS structures is primarily evaluated by the output voltage of the readout circuit, which is proportional to the travel distance of the movable bottom membrane.[12] In theoretical models, the shock is assumed to be a half-sine profile, similar to the shape of an actual shock pulse.[11,13] Furthermore, the frequency of mechanical shock usually spans from several hertz to 10 kHz[25] whereas the duration of the shock load varies from 0.1 to 1 millisecond, which mostly spans the duration of the shock pulse for a hard-floor drop test.[11]

MEMS device responses to the shock load can be analyzed either from the time history of the system (time domain approach) or through the shock response spectrum (frequency domain approach).[11] Figures 3(a) and 3(b) depict the temporal profiles of the output of the circuit upon external shock of approximately 100 g, (a) without and (b) with electrostatic force between top and bottom membranes. The movable bottom membrane travels towards the substrate due to inertia. By deploying merely 0.565 V between top and bottom membranes, the peak-to-peak amplitude decreases from 169.15 mV to 98.85 mV, resulting in 41.5% reduction. This mitigation method remains effective as well when the microstructure is exposed to both an external shock and an acoustic wave. Figures 3(c) and 3(d) show the microstructure movement generated amplitude of 231.7 mV (c) without any electrostatic force and (d) the amplitude decreases to 151.47 mV, which corresponds to a 34.6% reduction by applying 0.565 V between top and bottom membranes. Higher applied potentials between the top and bottom membrane are also tested under shock, and the resulting peak amplitudes are plotted as a function of applied voltage as shown in Fig. 3(g). As the electrostatic potential increases, the amplitude of the device decreases.

The electrostatic force between the top and bottom membranes works together with the inherent restoration force of the bottom membrane. Electrostatic force is inversely proportional to the effective gap distance and proportional to the effective area of membranes. Inherent restoration force, strongly correlated with the spring constant, is proportional to the thickness of the membranes. However, in practice, the spring constant of the thin film is largely dominated by the stress developed inside the thin film. We believe that the thin film stress may be responsible for the discrepancies between theoretical estimation and experimental results.

The effectiveness of shock-mitigation can be better illustrated by referring to the shock response in the frequency domain. The obvious distinction of the acoustic wave signal from the shock response signal makes the data analysis easier. By using a digital filter to filter out the 5 kHz acoustic wave signal, the amplitude of shock is decreased from 205.79 mV [Fig. 3(e) no electrostatic force] to 121.14 mV

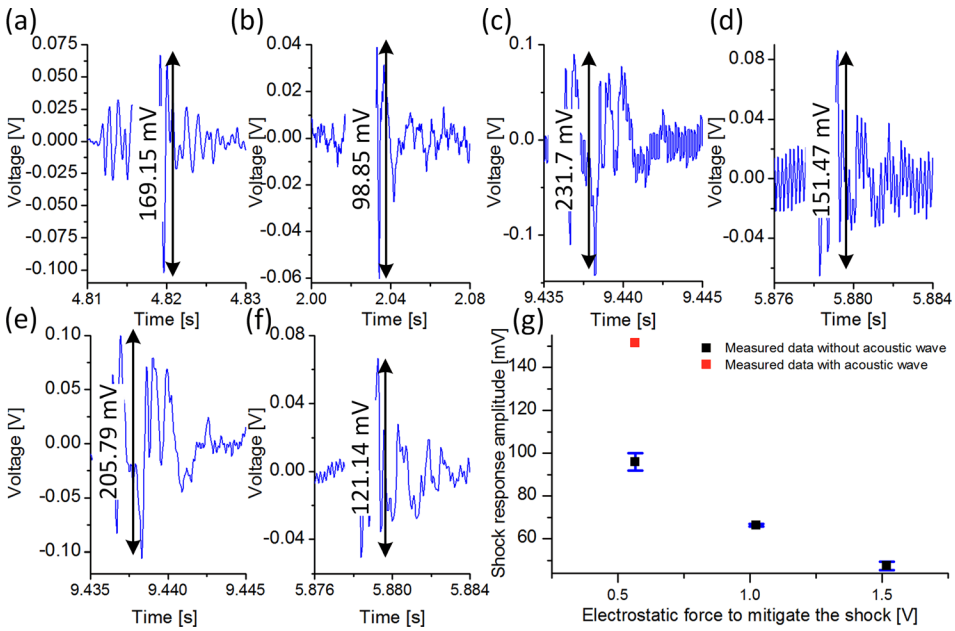

FIG. 3. *Ex-situ* control of shock-mitigation. (a) Shock response without mitigation. (b) Shock response with mitigation reduced the membrane travel distance by 41.5% using 0.565 V. (c) Shock response without mitigation in the presence of the 5 kHz acoustic signal. (d) Shock response with mitigation reduced the membrane travel distance by 34.6% using 0.565 V in the presence of the 5 kHz acoustic signal. Output of the dual-membrane structure. Shock load, 100 g; filtered out acoustic stimulus, 5 kHz. (e) Without any electrostatic force and (f) with 0.565 V between the top and bottom membranes, respectively. (g) Shock response amplitude as a function of electrostatic forces, 0.565 V, 1.023 V, and 1.517 V.

[Fig. 3(f) 0.565 V between the two membranes] by 41% reduction, which has a good agreement with the results shown in Figs. 3(a) and 3(b). It is concluded that our dual-membrane MEMS structure has capacity to mitigate the external shock load effectively under the influence of the acoustic wave stimulus, which meets the modeling purpose to be microphones in cell phones.

Similar to the *ex-situ* control, the peak shock amplitude decreases, and the mitigation becomes more effective as the electrostatic force increases. The reduction in the shock response with the increasing electrostatic force between the top and bottom membranes is shown in Fig. 4.

We present a shock mitigating technique, using a dual-membrane microstructure, which effectively attenuates the effects of external disturbances such as mechanical shock on a MEMS device. An *in-situ* shock mitigation configuration consists of an accelerometer and a shock mitigating controller; the accelerometer senses the shock and triggers the dual membrane structure to apply the electrostatic force to reduce the shock impact. To replicate real life settings, the shock-mitigation method triggers naturally based on conditions measured from the accelerometer and during acoustic excitation on the device. Our shock-mitigated theme may be used in microphones of cell phones. We used an off-the-shelf cost-effective accelerometer which is often adopted in a smart phone, having in mind that no additional components are added to embed our unique method for cell phone applications. Our shock-mitigated theme can be adopted other than cell phones as well, including capacitive MEMS structures that demand robust operation against external mechanical disturbances. The shock-mitigated method comprises a simple structure, uses CMOS-compatible materials and manufacturing process, and delivers a highly effective shock mitigation through low voltage electrostatic actuation. This dual membrane MEMS structure better than current MEMS devices, providing a shock mitigating profile necessary to maintain the device's functionality.

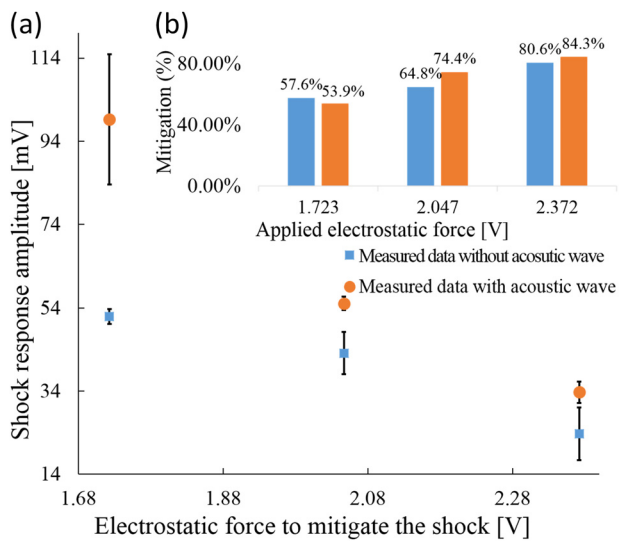

FIG. 4. *In-situ* control of shock-mitigation: (a) Shock response with different electrostatic forces, 1.723 V, 2.047 V, and 2.372 V. (b) Shock mitigation percentage versus applied electrostatic force between the top and bottom membranes.

The authors appreciate the support from National Science Foundation (ECCS-1101797).

[1]R. S. Shawgo, A. C. Richards Grayson, Y. Li, and M. J. Cima, "BioMEMS for drug delivery," Curr. Opin. Solid State Mater. Sci. **6**(4), 329–334 (2002).
[2]D. S. Eddy and D. R. Sparks, "Application of MEMS technology in automotive sensors and actuators," Proc. IEEE **86**(8), 1747–1755 (1998).
[3]L. Soyoon and B. Hyokyung, "Data allocation in MEMS-based mobile storage devices," IEEE Trans. Consum. Electron. **52**(2), 472–476 (2006).
[4]R. Oboe, R. Antonello, E. Lasalandra, G. S. Durante, and L. Prandi, "Control of a Z-axis MEMS vibrational gyroscope," IEEE/ASME Trans. Mechatronics **10**(4), 364–370 (2005).
[5]F. Hu, J. Yao, C. Qiu, and H. Ren, "A MEMS micromirror driven by electrostatic force," J. Electrostatics **68**(3), 237–242 (2010).
[6]R. Hao, T. Fenggang, W. Weimin, and Y. Jun, "An out-of-plane electrostatic actuator based on the lever principle," J. Micromech. Microeng. **21**(4), 045019 (2011).
[7]I. Deligoz, S. R. Naqvi, T. Copani, S. Kiaei, B. Bakkaloglu, S. S. Je, and J. Chae, "A MEMS-based power-scalable hearing aid analog front end," IEEE Trans. Biomed. Circuits Syst. **5**(3), 201–213 (2011).

[8]S. S. Je and J. Chae, "A compact, low-power, and electromagnetically actuated microspeaker for hearing aids," IEEE Electron Device Lett. **29**(8), 856–858 (2008).
[9]S.-S. Je, J. Kim, J. C. Harrison, M. N. Kozicki, and J. Chae, "In situ tuning of omnidirectional microelectromechanical-systems microphones to improve performance fit in hearing aids," Appl. Phys. Lett. **93**(12), 123501 (2008).
[10]Y. Yongmo and C. Junseok, "Miniaturized protein separation using a liquid chromatography column on a flexible substrate," J. Micromech. Microeng. **18**(12), 125010 (2008).
[11]M. I. Younis, F. Alsaleem, and D. Jordy, "The response of clamped–clamped microbeams under mechanical shock," Int. J. Non-Linear Mech. **42**(4), 643–657 (2007).
[12]G. X. Li and F. A. Shemansky, Jr., "Drop test and analysis on micromachined structures," Sens. Actuators, A **85**(1–3), 280–286 (2000).
[13]V. T. Srikar and S. D. Senturia, "The reliability of microelectromechanical systems (MEMS) in shock environments," J. Microelectromech. Syst. **11**(3), 206–214 (2002).
[14]D. M. Tanner, J. A. Walraven, K. Helgesen, L. W. Irwin, F. Brown, N. F. Smith, and N. Masters, "MEMS reliability in shock environments," in Proceedings of IEEE 38th Annual International Reliability Physics Symposium (2000).
[15]T. Niels, S. Tonny, J. Henri, L. Rob, and E. Miko, "Stiction in surface micromachining," J. Micromech. Microeng. **6**(4), 385 (1996).
[16]B. B. Lim, J. P. Yang, S. X. Chen, J. Q. Mou, and Y. Lu, "Shock analysis of MEMS actuator integrated with HGA for operational and non-operational HDD," in Magnetic Recording Conference on Digest of the Asia-Pacific, 2002.
[17]F. Alsaleem, M. I. Younis, and R. Miles, "An investigation into the effect of the PCB motion on the dynamic response of MEMS devices under mechanical shock loads," J. Electron. Packag. **130**(3), 031002-031002-10 (2008).
[18]M. I. Younis, D. Jordy, and J. M. Pitarresi, "Computationally efficient approaches to characterize the dynamic response of microstructures under mechanical shock," J. Microelectromech. Syst. **16**(3), 628–638 (2007).
[19]S. Subramanian, T. Maurizio, T. Branislav, L. Robert, O. Thomas, P. S. Ross, and R. S. Herbert, "Vibration and shock reliability of MEMS: Modeling and experimental validation," J. Micromech. Microeng. **21**(4), 045022 (2011).
[20]C. Yang, B. Zhang, D. Chen, and L. Lin, "Drop-shock dynamic analysis of MEMS/package system" in 2010 IEEE 23rd International Conference on Micro Electro Mechanical Systems (MEMS).
[21]L. B. Wilner, "A high performance variable capacitance accelerometer," in 5th IEEE Instrumentation and Measurement Technology Conference, Conference Record 1988 (IMTC-88), 1988.
[22]S. W. Yoon, N. Yazdi, N. C. Perkins, and K. Najafi, "Micromachined integrated shock protection for MEMS," Sens. Actuators A: Phys. **130–131**, 166–175 (2006).
[23]M. W. Weber, "Adaptive circuits and methods for reducing vibration or shock induced errors in *inertial sensors*," US7401515 B2 (2008).
[24]Q. Chen, Y.-C. Lai, J. Chae, and Y. Do, "Anti-phase synchronization in microelectromechanical systems and effect of impulsive perturbations," Phys. Rev. B **87**(14), 144304 (2013).
[25]J. S. Wilson, *Sensor Technology Handbook* (Elsevier Science, 2004) .